PROCEEDINGS OF SPIE

SPIEDigitalLibrary.org/conference-proceedings-of-spie

Wave optics propagation code for multiconjugate adaptive optics

Brent L. Ellerbroek, Gregory Cochran

Brent L. Ellerbroek, Gregory Cochran, "Wave optics propagation code for multiconjugate adaptive optics," Proc. SPIE 4494, Adaptive Optics Systems and Technology II, (4 February 2002); doi: 10.1117/12.454784

SPIE.

Event: International Symposium on Optical Science and Technology, 2001, San Diego, CA, United States

Downloaded From: https://www.spiedigitallibrary.org/conference-proceedings-of-spie on 6/29/2018 Terms of Use: https://www.spiedigitallibrary.org/terms-of-use

A Wave Optics Propagation Code for Multi-Conjugate Adaptive Optics

B.L. Ellerbroek[a] and G.M. Cochran[b1]
[a]Gemini Observatory; [b]Reconstruction Concepts

ABSTRACT

We describe the purpose, theory, implementation, and sample results of a wave optics propagation simulation developed to study multi-conjugate adaptive optics (MCAQ) for 4-10 m class telescopes. This code was more specifically developed to assess the impact of diffraction effects and a variety of implementation error sources upon the performance of the Gemini-South MCAO system. These errors include: Hartmann sensing with extended and elongated laser guide stars, optical propagation effects through the optics and atmosphere, laser guide star (LGS) projection through the atmosphere, deformable mirror (DM) and wave front sensor (WFS) misregistration, and calibration for non-common path errors. The code may be run in either a wave optics or geometric propagation mode to allow the code to be anchored against linear analytical models and to explicitly evaluate the impact of diffraction effects. The code is written in MATLAB, and complete simulations of the Gemini-South MCAO design (including 3 deformable mirrors with 769 actuators, 5 LGS WFS with 1020 subapertures, 3 tip/tilt natural guide star (NGS) WFS, and 50 meter phase screens with 1/32nd meter resolution) are possible using a Pentium III but require 1 to 6 days. Sample results are presented for Gemini-South MCAO as well as simpler AO systems. Several possibilities for parallelizing the code for faster execution and the modeling of extremely large telescopes (ELT's) are discussed.

Keywords: Multi-conjugate adaptive optics, adaptive optics modeling, extremely large telescopes

1 INTRODUCTION

The subject of performance evaluation for multi-conjugate adaptive optics (MCAO) [1] has already received considerable attention. Numerous studies of predicted performance are now available, many of them using analytical methods [2, 3, 4, 5] that are generalizations of techniques previously used to evaluate simpler adaptive optics (AO) systems [6, 7, 8]. Monte Carlo simulations have also been used to estimate MCAO performance [9]. All of these methods have obtained broadly consistent results. This is not too surprising, since they are all based upon a common first-order model for the AO system and the turbulence-induced phase errors to be corrected. Some of the basic elements of this model include: Optical phase distortions obtained by geometric ray tracing through the atmosphere and optical system, wave front sensor measurements that are linear functions of these phase profiles summed with additive noise, and a perfectly aligned and calibrated AO system. These assumptions simplify the computation of optimal reconstruction algorithms and best-case performance estimates for an ideal MCAO system, but higher-fidelity models will soon be required to address a range of more involved issues as the design work on real MCAO systems progresses. Some of these issues include:

- The nonlinearities and dynamic range limitations of Shack Hartmann (SH) sensors and other wave front sensing approaches;
- Scintillation and diffraction effects in the optics and atmosphere;

[1]Further author information –
BLE: Email: bellerbroek@gemini.edu; Telephone: (808) 974-2575; Fax: (808) 935-9235
GMC: Email: gmcochran@compuserve.com; Telephone: (505) 837-1008

Adaptive Optics Systems and Technology II, Robert K. Tyson, Domenico Bonaccini, Michael C. Roggemann, Editors, Proceedings of SPIE Vol. 4494 (2002)
© 2002 SPIE · 0277-786X/02/$15.00

Downloaded From: https://www.spiedigitallibrary.org/conference-proceedings-of-spie on 6/29/2018
Terms of Use: https://www.spiedigitallibrary.org/terms-of-use

- Laser guide star (LGS) elongation, aberrations, and pointing errors;
- Deformable mirror (DM) and wave front sensor (WFS) misregistration errors;
- Non-common path wave front errors;
- WFS gain and bias calibration in the presence of the above; and
- AO control loop temporal dynamics.

We are now developing a Monte Carlo wave optics propagation simulation to investigate these higher-order effects. This paper provides a brief description of this simulation and presents a few sample results for the proposed Gemini-South MCAO configuration and simpler AO systems.

Recent advances in microprocessor performance have greatly reduced the drudgery involved in developing and applying a propagation simulation to model a very-high-order AO system on a large telescope. Some of the improvement in processor speed can be given back to allow the use of higher-level languages, such as MATLAB or IDL, that provide a much more efficient and flexible development environment at the expense of some reduction in efficiency. Very large simulation cases are still tractable using this approach. The Gemini-South MCAO simulation, for example, includes 3 DM's with a total of 769 actuators, 3 natural guide star (NGS) and 5 LGS WFS's with a total of 1026 subapertures, and 7 atmospheric phase screens with an extent of 52.5 meters and a spatial resolution of 3.125 or 6.25 centimeters. These cases can be run on a 1 GHz Pentium III with 768 Mbytes of RAM, although the ratio between computer time and simulated time is in the range from 10^5 to 5×10^6, depending upon the range of simulation features included from the above list. This is still efficient enough to enable simulation runs to be completed in from a few hours to less than a week. These simulation results can be used to help quantify the impact of many MCAO system design parameters (e.g. the allowable DM-to-WFS misregistration) and increase confidence in MCAO performance predictions before the system is actually built. The significant costs and predicted high payoffs associated with implementing MCAO on 8 to 10 meter class telescopes make detailed and accurate modeling particularly important. This will be even more true for extremely large telescopes (ELT's), where wave optics propagation simulations of MCAO should still be possible using parallel processing.

The remainder of the paper is organized as follows. Section 2 is a qualitative overview of the features included in the simulation code. Section 3 is a brief summary of the steps in each simulation run, and Section 4 describes some of the basic mathematical models used for simulation operations such as optical propagation and Shack-Hartmann wave front sensing. Section 5 presents sample simulation results for both a conventional AO system and the LGS MCAO design under consideration for Gemini-South. Section 6 concludes with a few comments on how this work might be extended to consider ELT's.

2 SIMULATION OVERVIEW

Figure 1 is a schematic/cartoon illustrating the principal features included in the simulation. Atmospheric turbulence is modeled by one or more discrete, translating, periodic phase screens with approximately Kolmogorov or von Karman statistics. Optical propagation through the atmosphere can be modeled via either geometric ray tracing or wave optics, the latter implemented via a standard near field FFT propagator. Guide star constellations may be defined to include one or several NGS and one or several LGS at a common range. All guide stars within each of these classes currently share common magnitude and WFS characteristics. Laser guide stars may be modeled as either point or extended sources, with the shape of the latter depending upon the initial laser beam profile, the aberrations induced by the uplink propagation, and the vertical distribution of the backscatter layer. AO system performance is evaluated in terms of the mean point spread function and Strehl ratio time history at one or several points in the field-of-view.

Downloaded From: https://www.spiedigitallibrary.org/conference-proceedings-of-spie on 6/29/2018
Terms of Use: https://www.spiedigitallibrary.org/terms-of-use

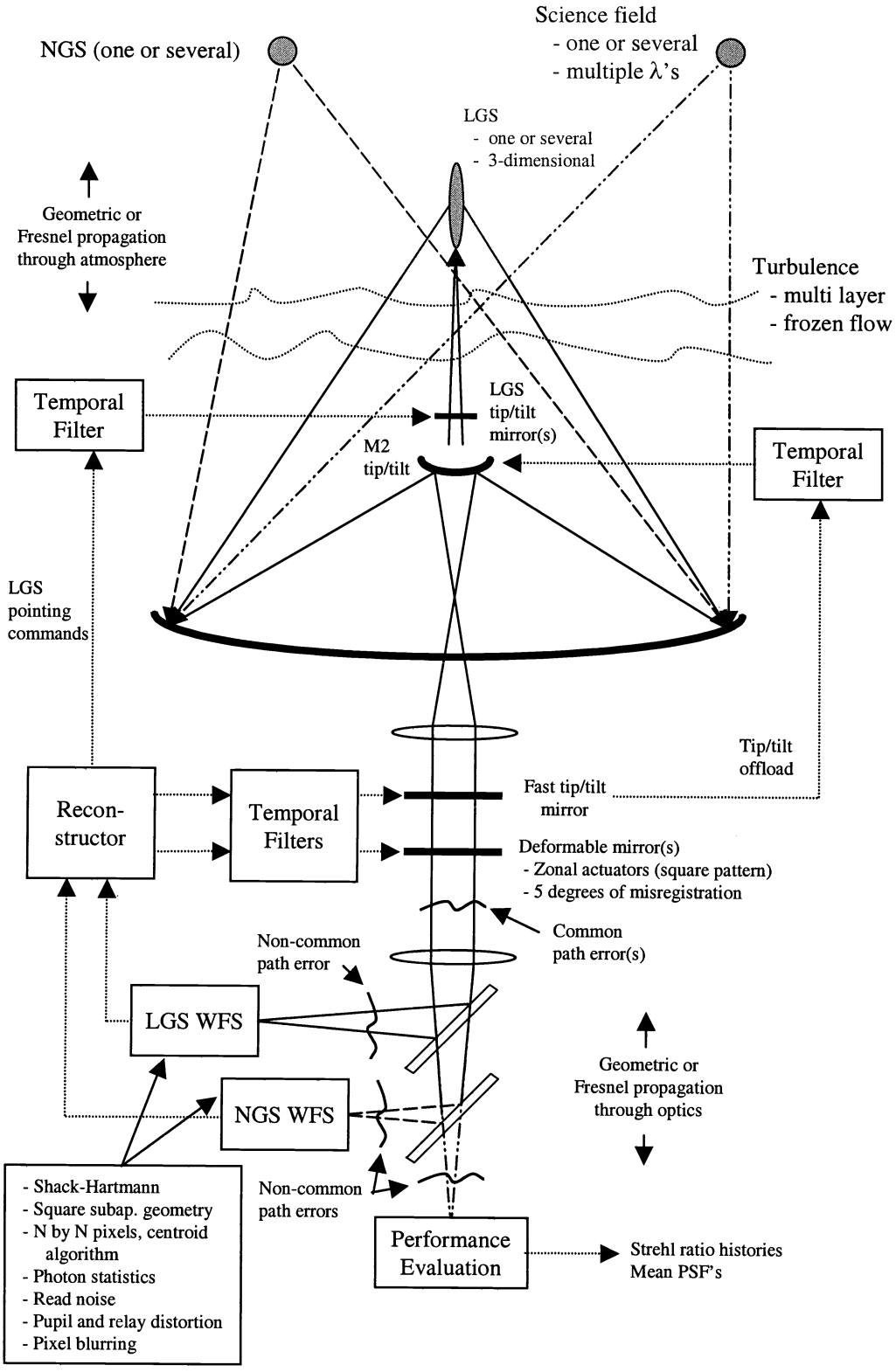

Figure 1: Simulation Features
This schematic/cartoon illustrates the basic features of the wave optics propagation simulation.

Downloaded From: https://www.spiedigitallibrary.org/conference-proceedings-of-spie on 6/29/2018
Terms of Use: https://www.spiedigitallibrary.org/terms-of-use

The telescope and AO system are modeled as one or more additional phase screens beginning with the telescope primary mirror. Each surface is defined in terms of a conjugate range, an amplitude transmittance profile, and a phase profile. The phase profile may include static figure errors and the dynamic adjustments applied to deformable and tip-tilt mirrors. Optical propagation from surface to surface is implemented using the same propagator as used for the atmosphere. The propagation path for each WFS and evaluation field point may also include a non-common path phase screen conjugate to the telescope entrance pupil.

The phase correctors currently modeled include two-axis tip/tilt mirrors and "zonal" deformable mirrors with a square actuator pattern. This pattern may be misaligned in five degrees of freedom (x- and y translation, rotation, and x- and y magnification) with respect to the ideal. Wave front sensors are currently limited to SH sensors with square actuator geometries. This geometry may be arbitrarily distorted with respect to an ideal square pattern to simulate pupil distortion. Each SH lenslet array is optically conjugate to the pupil of the telescope. WFS measurements may be modeled either geometrically as the average wavefront gradients over each subaperture, or as centroids computed from guide star images as recorded by cells of n by n pixels behind each lenslet in the SH array. Photon and detector read noise may be included in the pixel values. Laser guide star images are modeled isoplanatically by convolving the guide star intensity distribution in the sodium layer with a subaperture PSF computed for a point source at the average range of the layer. The raw centroids are gain- and bias calibrated to account for non-common path phase errors, the nominal atmospheric seeing, and the nominal intensity distribution of the LGS.

The actuator commands to each DM and tip/tilt mirror (TTM) are computed using a minimal variance reconstruction algorithm as previously described [3]. The reconstructed actuator estimates are temporally filtered by a discrete finite difference equation before they are applied to the active mirrors, with two separate sets of coefficients specifiable for the DM's and the TTM. Actuator temporal dynamics are modeled as a damped harmonic oscillator. The fast tip/tilt mirror may be offloaded to a second slow tip/tilt mirror (such as the telescope secondary mirror). LGS pointing mirrors may also be driven to null the average tilt measurement from each LGS WFS. The overall control system architecture is quite standard, but other approaches, such as modal or predictive control, could be simulated with relatively modest modifications to the code.

Some of the features presently not modeled include (i) windshake and other dynamic errors in the optical system, (ii) DM actuator hysteresis and finite dynamic range, (iii) advanced or nonstandard control algorithms, and (iv) background noise from either the sky or Rayleigh backscatter.

3 SIMULATION SEQUENCE

This section gives a brief summary of the sequence of processing steps that comprise a single simulation run.

3.1 Parameter definition

The user-input parameters that specify the scenario to be simulated are divided into seven categories: General parameters (simulation length, phase screen size and resolution, etc.), atmospheric model, performance evaluation directions and wavelengths, telescope optical surfaces, WFS parameters, DM and TTM parameters, and control algorithm parameters. These values are defined, stored, and modified using a simple menu-driven interface.

Downloaded From: https://www.spiedigitallibrary.org/conference-proceedings-of-spie on 6/29/2018
Terms of Use: https://www.spiedigitallibrary.org/terms-of-use

3.2 Scenario Generation

This step builds most of the data structures describing the AO system and the atmosphere, including the following quantities:

- The telescope clear aperture function.
- Amplitude and phase profiles for the remaining optical surfaces in the telescope and the LGS laser beams. These functions are input from files that have been precomputed by the user.
- DM actuator locations and influence functions.
- DM commands to minimize the residual static aberrations in the science path. These commands are computed to minimize the mean-square wavefront error over the set of evaluation directions, assuming perfect knowledge of the non common path errors.
- WFS subaperture locations and geometric "influence functions."
- WFS biases and gains.
- The Geometric DM-to-WFS influence matrix. This will be used to compute the reconstruction algorithm.
- The simulation event list (see section 3.4 below).
- Atmospheric phase screens.
- The initial (zeroed) state of the AO control loops.

The simulation starting conditions are saved to a file to simplify setting up multiple runs with slight variations to the parameters (e.g., selecting geometric or wave-optics propagation with all other parameters held constant).

3.3 Reconstructor Computation

The wavefront reconstruction matrix is computed to minimize the field- and aperture averaged mean-square residual wavefront error over the set of evaluation directions specified by the user in subsection 3.1 above. The simulation generates an input file for an existing FORTRAN program that computes the reconstruction matrix and estimates AO performance assuming geometric propagation and no misregistration or non common path errors. For simulations including a separate tip/tilt mirror, the reconstruction matrix is decomposed into separate components for the DM's and the TTM.

3.4 Time Domain Simulation

The Monte Carlo simulation proper is driven by an event list that describes the order of execution of a set of high-level operations that are the building blocks of the simulation time line. Each element of the list comprises an event type, the time for the initial occurence of the event, the repetition interval, and one or several event-specific parameters. The simulation driver repeatedly scans through this list, locates and executes the next event to occur, and increments the time of that event by its repetition interval. This approach allows a wide range of timelines to be simulated by simple adjustments to the scenario input parameters. The currently implemented set of events includes:

Downloaded From: https://www.spiedigitallibrary.org/conference-proceedings-of-spie on 6/29/2018
Terms of Use: https://www.spiedigitallibrary.org/terms-of-use

- Evaluate performance: Loop over the evaluation directions and wavelengths. For each direction and wavelength, propagate a plane wavefront from infinity through each atmospheric phase screen and optical surface, with each phase profile computed at the current time using either the Taylor hypothesis (for atmospheric phase screens) or the damped harmonic oscillator model (for DM's and the TTM). Propagate to the far field, record the Strehl ratio, and accumulate the mean PSF.

- Accumulate signal for WFS class i: The class i equals either 1 or 2 for the NGS or LGS WFS measurements. Loop over the guide star directions and (for polychromatic NGS) wavelengths. For each direction and wavelength, propagate a plane or spherical wavefront from the guide star through each atmospheric phase screen and optical surface, with each phase profile computed at the current time. Compute the instantaneous WFS measurement, either in terms of subaperture-averaged wavefront gradients or the subaperture PSFs on the Shack-Hartmann array. For laser guidestars, propagate the laser beam up through the atmosphere (at the appropriate earlier point in time), and convolve each subaperture PSF with the LGS intensity distribution in the sodium layer. Add the instantaneous WFS signal (either mean wavefront gradient or pixel intensities) to the accumulated signal for the current integration interval. (Accumulating multiple WFS measurements during each integration interval improves the modeling of control loop temporal dynamics, but this feature has not been exercised for any of the results presented in this paper).

- Readout WFS class i: For geometric simulations, add measurement noise to each accumulated gradient measurement and zero the accumulated measurements for the next integration interval. For wave optics simulations, add photon and detector noise to each pixel, compute SH spot centroids from the noisy pixel values, and zero the accumulated measurements for the next integration interval. Apply gain and bias calibration to the measurements in either case (although the gain calibration is always unity for geometric simulations).

- Update DM actuator commands: Compute the current values of the DM actuator positions from their positions at the previous cycle, the commands applied at the beginning of the previous cycle, and the damped harmonic oscillator model. Multiply the most current set of WFS measurements by the DM reconstruction matrix, and filter the estimated actuator errors by the DM finite difference equation to determine the new set of actuator commands. The new actuator commands and positions will be used to compute the figures of the deformable mirrors for any optical propagations that occur between this time and the next DM command update.

- Update fast TTM commands: This is similar to updating the DM actuator commands, except that the TTM parameters are used for the values of the reconstruction matrix, the finite difference equation, and the damped harmonic oscillator model.

- Offload the fast TTM to the slow TTM: Compute the current positions of the slow TTM actuators as above. Compute the new commands to the slow TTM actuators, using the current commands to the fast TTM as the error signals to the slow TTM finite difference equation.

- Update the LGS pointing mirror commands: Compute the current positions of the LGS pointing mirror actuators as above. Compute the new commands to the pointing mirrors, using the average tilt measurement from each LGS WFS as the error signal to the pointing mirror finite difference equation.

- Stop: Exit the simulation loop.

3.5 Postprocessing

At present, this step simply averages the accumulated PSFs to determine the mean PSF for each evaluation direction and wavelength, and then outputs these mean PSFs and the Strehl ratio time histories to a file for later analysis. It is relatively straightforward to augment these two quantities with additional data (e.g., the DM actuator commands at each simulation cycle) on a case-by-case basis for either debugging purposes or a more detailed analysis of AO loop performance.

Downloaded From: https://www.spiedigitallibrary.org/conference-proceedings-of-spie on 6/29/2018
Terms of Use: https://www.spiedigitallibrary.org/terms-of-use

4 SIMULATION MODELS

This section describes in somewhat greater detail the basic mathematical models for some of more fundamental quantities used and operations performed by the simulation. Readers should be careful not to assume continuity of notation across subsection boundaries.

4.1 Phase Screen Generation

The simulation computes atmospheric phase screen realizations as spatially filtered white noise according to the formula

$$\mathrm{OPD}(\vec{x}) = c\,\Re\left\{\mathcal{F}\left[\sqrt{\Phi(\vec{\kappa})}\,(r(\vec{\kappa}) + ir'(\vec{\kappa}))\right]\right\}, \tag{1}$$

where OPD is the phase screen, $\mathcal{F}$ is the 2-dimensional spatial Fourier transform, Φ is the spatial power spectrum of the turbulence, $\vec{\kappa}$ is a spatial frequency variable, r and r' are zero mean, unit variance, real-valued white noise functions, and c is a scaling factor for the strength of the screen. For a von Karman turbulence spectrum, the function Φ takes the form

$$\Phi(\vec{\kappa}) = \left|\kappa^2 + (W/L_0)^2\right|^{-11/6}, \tag{2}$$

where W is the width of the phase screen and L_0 is the turbulence outer scale. Setting $L_0 = \infty$ yields the usual Kolmogorov spectrum. Finally, the constant c is defined by the expression

$$c = 0.1517\sqrt{f}\left(\frac{W}{r_0}\right)^{5/6}\left(\frac{\lambda}{2\pi}\right), \tag{3}$$

where f is the fraction of the integrated atmospheric turbulence strength in the layer, and r_0 is the turbulence-induced coherence diameter at wavelength λ. This definition for the scaling factor c yields a phase screen expressed as an optical path difference, not as radians of phase at a particular wavelength.

Eq. (1) is implemented via a fast Fourier transform (FFT), and the resulting phase screens are periodic. The width W of the phase screen must therefore be considerably larger than the telescope aperture diameter, and it should ideally also be large compared to the turbulence outer scale. The amount of turbulence in low-order modes will be underestimated if this second condition is not satisfied. Sample results in Section 5 below illustrate that performance estimates for closed loop AO are generally not a very strong function of the outer scale or the width of the phase screens, however.

4.2 Optical Propagation

Wave optics propagation from plane to plane is modeled as a spatial filtering operation, namely

$$U_{n+1}(\vec{x}) = \mathcal{F}\left[\exp(i\pi\kappa^2\lambda z)\mathcal{F}^{-1}\left(U_n(\vec{y})S_n(\vec{y})\right)\right](\vec{x}). \tag{4}$$

Here U_n is the optical field immediately before encountering the (multiplicative) phase screen S_n at layer number n, $\mathcal{F}$ is still the two-dimensional spatial Fourier transform operator, λ is the wavelength, and z is the distance from layer n to layer $n+1$. The complex field U_n is related to the amplitude a and phase ϕ of the beam by the equation

$$U_n(\vec{x}) = a_n(\vec{x})\exp(i\phi_n(\vec{x})), \tag{5}$$

and the complex phase screen S_n is similarly related to the optical path difference OPD_n and amplitude transmittance function t_n:

$$S_n(\vec{x}) = t_n(\vec{x})\exp(2\pi i\mathrm{OPD}_n(\vec{x})/\lambda) \tag{6}$$

Downloaded From: https://www.spiedigitallibrary.org/conference-proceedings-of-spie on 6/29/2018
Terms of Use: https://www.spiedigitallibrary.org/terms-of-use

The transmittance function t_n is used to define the telescope clear aperture, and possibly other aperture and/or field stops within the optical system.

Eq. (4) may be used for both upwards and downwards propagation though both the atmosphere and optics. The initial field U_0 is a infinite flat or spherical wavefront at the top of the atmosphere for downwards propagation, and is equal to the laser beam profile at the launch telescope for LGS propagation up through the atmosphere. The propagation distance z is treated as positive in both cases, except in the event that an optical relay forms an image of a plane located earlier along the propagation path. This occurs in an MCAO system, for example, when a wavefront propagates from the telescope aperture to a deformable mirror optically conjugate to a nonzero altitude.

Eq. (4) cannot be implemented exactly as written using FFT's, since the input field U_0 will oscillate extremely rapidly for a guide star that is off-axis or at finite range due to the resulting linear (tilt) and quadratic (focus) terms present in the phase function ϕ_0. The case of an off-axis star may be treated by defining a new coordinate system with the z axis parallel to the direction of propagation. Making a paraxial approximation, the propagation equation now becomes

$$U_{n+1}(\vec{x} + z_{n+1}\vec{\theta}) = \mathcal{F}\left[\exp(i\pi\kappa^2\lambda z)\mathcal{F}^{-1}\left(U_n(\vec{y} + z_n\vec{\theta})S_n(\vec{y} + z_n\vec{\theta})\right)\right](\vec{x}), \tag{7}$$

where $\vec{\theta}$ is the direction of the source, and z_n and z_{n+1} are the z coordinates of the two layers. Eq. (7) may also be obtained by explicitly identifying the nominal tilt term $2\pi\vec{\theta}\cdot\vec{x}/\lambda$ in the wavefront ϕ_n and applying the Fourier shift theorem. For numerical calculations, the values of the phase screen S_n will need to be interpolated except in the very special case that the offset $z_n\vec{\theta}$ is exactly divisible by the simulation grid spacing. Our subjective experience is that this interpolation is best performed via the Fourier shift theorem,

$$S_n(\vec{x} + z_n\vec{\theta}) = \mathcal{F}\left[\exp(-2\pi i z_n\vec{\theta}\cdot\vec{\kappa})\mathcal{F}^{-1}\left(S_n(\vec{y})\right)\right](\vec{x}), \tag{8}$$

since linear and even cubic spline interpolation will amplify the high spatial frequency content of the screen. The same technique can be used to translate phase screens with time according to the Taylor (frozen flow) hypothesis, and in fact the net effect of these two operations can be implemented in a single step.

For a guide star located at a finite range z_f, the propagation equation is further modified to take the form

$$U_{n+1}\left[\left(\frac{z_f - z_{n+1}}{z_f - z_n}\right)\vec{x} + z_{n+1}\vec{\theta}\right] = \mathcal{F}\left\{\exp\left[i\pi\kappa^2\lambda z\left(\frac{z_f - z_n}{z_f - z_{n+1}}\right)\right]\mathcal{F}^{-1}\left(U_n(\vec{y} + z_n\vec{\theta})S_n(\vec{y} + z_n\vec{\theta})\right)\right\}(\vec{x}), \tag{9}$$

where the nominal spherical term of the wavefront ϕ_n is also dropped in this expression. One way to derive this expression is to propagate both S_nU_n and U_{n+1} to the plane $z = z_f$ with no intervening phase aberrations using the usual far field propagator [11], and set the two results equal. Solving this relationship for U_{n+1} yields Eq. (9).

Because of the scale factor appearing before $\vec{x}$ on the left hand side of Eq. (9), the fields U_n and U_{n+1} will be evaluated on two different meshes when the propagation equation is implemented using FFT's. The mesh spacing for each screen is proportional to the distance from the screen to the focal plane at $z = z_f$, so Eq. (9) is sometimes described as using a converging coordinate system. This is significant for simulation purposes because the atmospheric screens S_n must now be evaluated on two different meshes for the LGS and NGS propagations. It is much more computationally efficient to interpolate each screen only once and save the results if sufficient memory is available.

4.3 Active Mirrors

Deformable- and tip-tilt mirror phase adjustments are modeled using the usual linear superposition approximation,

$$\mathrm{OPD}(\vec{x}) = \sum_i p_i h_i(\vec{x}), \tag{10}$$

Downloaded From: https://www.spiedigitallibrary.org/conference-proceedings-of-spie on 6/29/2018
Terms of Use: https://www.spiedigitallibrary.org/terms-of-use

where p_i is the position (displacement) of actuator number i, and $h_i(\vec{x})$ is the influence function for that actuator. Hysteresis and saturation effects are not considered at this time. For deformable mirrors, the influence function h_i is a simple two-dimensional linear spline, with the actuators nominally located on a square grid. The actuator locations may be misaligned in x- and y displacement, rotation, and $x-$ and y magnification. The influence functions will be similarly distorted in this case.

The position of each actuator is determined according to the differential equation

$$c(t) = kp(t) + dp'(t) + mp''(t), \tag{11}$$

where $c(t)$ is the (position) command to the actuator, and the coefficients k, d, and m describe the dynamics of a damped harmonic oscillator. This model is used for the deformable mirrors, the fast tip/tilt mirror, the slow tip/tilt mirror, and the LGS pointing mirrors, although different coefficients may be defined for each mirror class. One method for solving Eq. (11) is to transform it into the form

$$\vec{x}'(t) = A\vec{x}(t) + B(t), \tag{12}$$

which may be solved using Laplace transforms with the result

$$\begin{aligned} \vec{x}(t) &= e^{At}\vec{x}(0) + A^{-1}(e^{At} - I)B \\ &= U\left[e^{\Lambda t}U^{-1}\vec{x}(0) + \Lambda^{-1}(e^{\Lambda t} - I)U^{-1}B\right], \end{aligned} \tag{13}$$

where

$$A = U\Lambda U^{-1}, \tag{14}$$

is the eigenvalue-eigenvector decomposition of the matrix A. If $m = 0$, then the required variable transformation is just $x(t) = p(t)$, $A = -k/d$, and $B = c/d$. If m is nonzero, these definitions become

$$\vec{x}(t) = \begin{pmatrix} p(t) \\ p'(t) \end{pmatrix} \tag{15}$$

$$A = \begin{pmatrix} 0 & 1 \\ -k/m & -d/m \end{pmatrix} \tag{16}$$

$$B = \begin{pmatrix} 0 \\ c/m \end{pmatrix} \tag{17}$$

4.4 Image Formation

The simulation uses the usual propagation equation to compute the far-field point spread function (PSF) associated with an optical field U,

$$\mathrm{PSF}(\vec{\theta}) = \left|\mathcal{F}(U(\vec{x}))\right|^2 (\vec{\theta}/\lambda). \tag{18}$$

This same equation is used to compute Shack-Hartmann spots and laser guide star intensity distributions as described further below.

4.5 Wavefront Sensing

For geometric simulations, we use the usual first order approximation for the wavefront gradient (or slope) measurement $\vec{s}$ obtained from a Shack-Hartmann sensor:

$$\vec{s} = \left[\int d\vec{x}\, W_{sa}(\vec{x})\right]^{-1} \int d\vec{x}\, W_{sa}(\vec{x}) \nabla \mathrm{OPD}(\vec{x}) + \vec{n} \tag{19}$$

Downloaded From: https://www.spiedigitallibrary.org/conference-proceedings-of-spie on 6/29/2018
Terms of Use: https://www.spiedigitallibrary.org/terms-of-use

Here W_{sa} defines the areas of the subaperture, ∇ is the gradient operator, OPD is the input wave front expressed as an optical path difference, and $\vec{n}$ is additive white noise.

For wave optics simulations, each subaperture tip/tilt measurement from the SH WFS is modeled as a centroid computed from noisy measurements of the subaperture Shack-Hartmann spot. The formula for the gradient $\vec{s}$ on a single subaperture becomes

$$\vec{s} = g^{-1}\left[\left(\sum_i c_i \vec{p}_i / \sum_i c_i\right) - \vec{b}\right], \tag{20}$$

where g and $\vec{b}$ are gain and bias calibration factors computed as described below, c_i is the number of photodetection events (or counts) on pixel number i in the subaperture, and $\vec{p}_i$ are the focal plane coordinates of pixel number i (Quadrant detectors have been used in all simulations to date). The pixel output c_i is modeled as the sum of a Poisson process plus zero mean, normally distributed detector read noise. For a given input field incident upon the SH array, the mean value of c_i is described by the expression

$$\begin{aligned} \bar{c}_i &= \int d\vec{x}\, \bar{I}(\vec{x}) W_p(\vec{x} - \vec{p}_i) \\ &= \int d\vec{\kappa} \mathcal{F}(\bar{I})(\vec{\kappa}) \left[\mathcal{F}(W_p)(\vec{\kappa})\right]^* \exp(2\pi i \vec{p}_i \cdot \vec{\kappa}), \end{aligned} \tag{21}$$

where $\bar{I}$ is the probability density function for the Shack-Hartmann spot, W_p is the nominal responsivity function for a single detector, $\vec{p}_i$ is again the location of pixel number i, and the superscript "$*$" denotes complex conjugation. The second equality follows from the Plancheral theorem and the Fourier shift theorem, and is the formula actually implemented in the simulation.

For NGS wavefront sensing, the Shack-Hartmann spot is evaluated using the formula

$$\bar{I}(\vec{\theta}) \propto \mathrm{PSF}_{sa}(\vec{\theta}), \tag{22}$$

where the point spread function PSF_{sa} is computed from Eq. (18) with the optical field U multiplied by the subaperture transmittance function W_{sa}. For LGS wavefront sensing, this PSF must be convolved with the three-dimensional intensity profile of the LGS in the sodium layer:

$$\bar{I}(\vec{\theta}) \propto \mathrm{PSF}_{sa}(\vec{\theta}) * \mathrm{PSF}_{lb}(\vec{\theta}) * e(\vec{\theta}), \tag{23}$$

where PSF_{lb} is computed according to Eq. (18) with U equal to the laser beam intensity profile at the top of the atmosphere, and e is an elongation factor that is a function of the separation between the launch telescope and the subaperture. This one-dimensional elongation factor is given to first order by the expression

$$e(\vec{\theta}) = \delta(\vec{\theta} \cdot \vec{r}_\perp) d[\bar{z}(1 - \bar{z}\theta / r^{-1})]. \tag{24}$$

Here δ is the usual Dirac delta function, $\vec{r}$ is the separation between the launch telescope and the subaperture, $\vec{r}_\perp$ is a unit vector orthogonal to $\vec{r}$, $d(z)$ is the density of the sodium layer as a function of altitude, and $\bar{z}$ is the mean range to the sodium layer.

By using Eq. (23), we are implicitly assuming that (i) the shape of the two-dimensional LGS cross section is constant through the sodium layer, (ii) the extent of the guide star is small compared to the isoplanatic patch size for a subaperture, and (iii) the LGS WFS is correctly focused and boresighted with respect to the LGS. The constants of proportionality in Eq.'s (22) and (23) are set to yield the desired mean signal level for each SH subaperture. Transforming to the Fourier domain, Eq. (23) becomes

$$\mathcal{F}(\bar{I})(\vec{\kappa}) \propto \mathcal{F}(\mathrm{PSF}_{sa})(\vec{\kappa}) \mathcal{F}(\mathrm{PSF}_{lb})(\vec{\kappa}) \mathcal{F}(e)(\vec{\kappa}). \tag{25}$$

This expression for $\mathcal{F}(\bar{I})$ is used in Eq. (21) to compute mean signal levels for each WFS pixel.

Downloaded From: https://www.spiedigitallibrary.org/conference-proceedings-of-spie on 6/29/2018
Terms of Use: https://www.spiedigitallibrary.org/terms-of-use

It remains to describe the calculation of the gain and bias calibration coefficients g and $\vec{b}$. The bias $\vec{b}$ is equal to the centroid computed for a long-exposure SH spot that has been ensemble averaged over atmospheric turbulence statistics, and the gain g is computed by "scanning" this average spot across the SH detector array. Neglecting outer scale effects, the Fourier transform of a ensemble-averaged NGS SH spot is given by the expression

$$\left\langle \mathcal{F}(\bar{I})(\vec{\kappa}) \right\rangle \propto \mathcal{F}(\mathrm{PSF}_{sa,0})(\vec{\kappa}) \exp[-3.44(\lambda\kappa/r_0)^{5/3}], \tag{26}$$

where the angle brackets, $\langle \ldots \rangle$, denote averaging over turbulence statistics, r_0 is again the turbulence induced effective coherence diameter, and PSF_{sa_0} is the Shack-Hartmann spot computed for the wave front distortions present in the optical system without atmospheric turbulence effects. For LGS SH spots, the corresponding formula is

$$\left\langle \mathcal{F}(\bar{I})(\vec{\kappa}) \right\rangle \propto \mathcal{F}(\mathrm{PSF}_{sa,0})(\vec{\kappa}) \mathcal{F}(\mathrm{PSF}_{lb,0})(\vec{\kappa}) \mathcal{F}(e)(\vec{\kappa}) \exp[-6.88(\lambda\kappa/r_0)^{5/3}], \tag{27}$$

where $\mathrm{PSF}_{lb,0}$ is the far field intensity profile for the laser beam with no additional turbulence-induced phase errors. This last expression includes a factor of 6.88, not 3.44, in the long-exposure filter function because turbulence degrades both the LGS intensity distribution in the sodium layer and the WFS subaperture PSF. Any correlations between the effects of aberrations on the uplink and downlink are neglected in the calculation of g and $\vec{b}$, but not in the simulation itself.

4.6 Wavefront Reconstruction and Loop Filtering

For simulations without a separate tip/tilt mirror, the current error $\vec{e}$ in the DM actuator command vector is estimated using the equation

$$\vec{e} = E\vec{s}, \tag{28}$$

where E is the reconstruction matrix and $\vec{s}$ is combined WFS measurement vector. Full aperture wavefront tilt is projected off each individual LGS WFS measurement vector before the combined vector $\vec{s}$ is assembled. The reconstruction matrix E is computed by a separate analysis program using methods described previously [3]. It is derived assuming geometric optics and a Kolmogorov turbulence spectrum, using the DM-to-WFS influence matrix computed by the simulation code.

For simulations that do include a separate tip/tilt mirror, the DM and TTM actuator errors are computed in parallel using two separate reconstruction matrices by the formulas

$$\vec{e}_{dm} = P_{dm}E\vec{s} \tag{29}$$

$$\vec{e}_{ttm} = P_{ttm}E\vec{s} \tag{30}$$

The matrix P_{dm} simply removes the overall tip/tilt component from a DM actuator command vector, and P_{ttm} converts this tip/tilt component (or the sum of the components from multiple DM's) into corresponding tip/tilt mirror actuator commands.

The actuator error vectors are temporally filtered by finite difference equations to compute the commands applied to the deformable and tip/tilt mirrors. These filters are of the form

$$\vec{c}(n) = \sum_{i=1}^{n} a_i \vec{c}(n-i) + \sum_{i=0}^{n-1} b_{i+1} \vec{e}(n-i), \tag{31}$$

where $\vec{e}(n)$ is the error vector at cycle n, and $\vec{c}(n)$ is the resulting command vector. Signal processing latency can be simulated by shifting the coefficients b_i to a later time. Two separate sets of coefficients a_i and b_i may be specified for the tip/tilt and deformable mirrors. Similar equations are used to drive the slow tip/tilt mirror and the LGS pointing mirrors, except that the definitions for the error vectors $\vec{e}$ are somewhat different. For the slow tip/tilt mirror, the vector $\vec{e}$ is the current command to the fast tip/tilt mirror. For the LGS pointing mirrors, the vector $\vec{e}$ is comprised of the full aperture tip/tilt measurements on the LGS WFS.

Downloaded From: https://www.spiedigitallibrary.org/conference-proceedings-of-spie on 6/29/2018
Terms of Use: https://www.spiedigitallibrary.org/terms-of-use

5 SAMPLE RESULTS

In this section, we describe two sample simulation results to illustrate some of the capabilities of the code. The first result is for a low-order conventional AO system, and the second is for the MCAO design now under development for the Gemini-South telescope.

5.1 Servo Lag for a Conventional AO System

This is one of several fairly early simulation results obtained to verify the correctness and accuracy of the code. The simulated AO system consisted of an 8-meter telescope with 6 by 6 DM actuators and 5 by 5 SH WFS subapertures. The simulation used a 256 by 256 point propagation grid with a mesh of 0.2 meters, yielding a phase screen width of 51.2 meters. The simulation also used a single atmospheric phase screen in the aperture plane of the telescope, with the turbulence-induced effective coherence diameter, r_0, equal to 0.166 m at a wavelength of 0.5 μm. The WFS measurement noise level was set to zero, and there was no offset between the direction of the guide star and the evaluation direction. Additional simulations were also performed to evaluate the simulation's treatment of these other error sources.

The simulated servo control law was a pure integrator with one cycle of time delay. In the notation of Eq. (31), this control law is defined by the parameters $n = 1$, $a_0 = 1$, and $b_1 = g$, where g is referred to as the gain of the servo. One cycle of delay was modeled by evaluating performance immediately before the DM actuator command vector was updated, so that the correction applied at cycle n was scored against the atmospheric turbulence profile at cycle $n + 1$.

The simulation was run in geometric propagation mode, so that exact agreement between analytical and simulation results could in principal be achieved. The validity of the simulation was assessed by comparing Strehl ratios averaged over 100 simulation cycles against the analytical performance predictions. Exact agreement is too much to expect for several reasons. There is some randomness in the average results after only 100 iterations, there are slight numerical differences between the simulation and analytical models of the DM-to-WFS influence matrices, and the power spectra of the turbulence-induced phase errors are not identical between the two codes. In particular, the simulation phase screens are periodic, and have an effective outer scale of no greater than $51.2/2 = 25.6$ meters, even if the outer scale parameter L_0 is set to infinity. Simulation runs and analytical Strehl calculations were generated for both $L_0 = \infty$ and $L_0 = 25.6$ m to study the impact of this approximation.

The results obtained are summarized in Table 1. The overall level of agreement between the analytical and simulation Strehls is good, with differences consistently no greater than 1-3 per cent (absolute) for Strehls in the range from 0.07 to 0.60. The finite outer scale improved Strehls ratios by about 1-3 per cent (absolute) for both analysis and simulation. The analytical Strehl ratios for $L_0 = 25.6$ m and $L_0 = \infty$ bracket the simulation results for $L_0 = \infty$ in nearly all cases.

5.2 MCAO for Gemini-South

This subsection presents the first of a series of increasingly detailed simulation results obtained to validate the preliminary design of the MCAO system now under development for the Gemini-South telescope. The principal goal of these simulations was to understand how MCAO performance is influenced by higher-order effects such as diffraction, DM misregistration, and imperfect calibration for non-common path errors. See [12] for some of these additional simulations.

Table 2 lists the 7-layer discrete fit to the median Cerro Pachon atmospheric turbulence profile used for these

Downloaded From: https://www.spiedigitallibrary.org/conference-proceedings-of-spie on 6/29/2018
Terms of Use: https://www.spiedigitallibrary.org/terms-of-use

Wavelength, μm	Loop gain, g	Analysis Strehl		Simulation Strehl	
		$L_0 = 25.6\,\mathrm{m}$	$L_0 = \infty$	$L_0 = 25.6\,\mathrm{m}$	$L_0 = \infty$
1.65	1.00	0.183	0.205	0.207	0.230
	0.50	0.124	0.148	0.133	0.161
	0.33	0.076	0.097	0.077	0.104
2.20	1.00	0.380	0.406	0.410	0.436
	0.50	0.302	0.336	0.320	0.357
	0.33	0.221	0.261	0.232	0.278
2.90	1.00	0.571	0.594	0.598	0.619
	0.50	0.499	0.532	0.519	0.553
	0.33	0.414	0.458	0.429	0.479

Table 1: AO performance vs. AO loop Gain

The quantity g is the loop gain for a sampled data control law of the form $c(n+1) = ge(n+1) + c(n)$, where $c(n)$ is the DM actuator command vector at cycle n, and $e(n)$ is the reconstructed wavefront error.

Layer	Altitude, m	Fractional Strength	Windspeed, m/s
1	0	0.6475	5.0
2	2077	0.1111	10.0
3	3414	0.0774	15.0
4	5562	0.0439	20.0
5	7212	0.0245	30.0
6	13091	0.0810	20.0
7	15840	0.0146	10.0

Table 2: Atmospheric Turbulence and Windspeed Profiles

This profile is based upon median seeing conditions at Cerro Pachon. Note that the layer altitudes are expressed in terms of the altitude above the site.

MCAO simulations. The value of r_0 for this profile is 0.166 m at a wavelength of 0.5 μm, and the isoplanatic angle for this profile is approximately 2.75 arc seconds. Table 3 lists the geometrical AO system parameters used in the MCAO simulations. These values are equal the parameters for the Gemini-South MCAO design except as noted in the table caption. The simulation used a propagation grid mesh of 1/32 meter, a grid size of 1680 points, and a total grid width of 52.5 meters. The simulation ran for 100 cycles, with mean Strehl ratios averaged over cycles 11-100. We used the geometric propagation option at first so that simulation results could once again be validated against analytical performance predictions.

Table 4 summarizes the results obtained from the MCAO simulation. Strehl ratios are presented for J, H, and K bands (1.25, 1.65, and 2.2 microns), at the center, edge, and corner of a one square arc minute field of view. The edge and corner values are averaged over all four edges and corners. As before, the simulation Strehl ratios are slightly higher than the analytical calculations, but consistently agree to within 1-3 per cent.

Downloaded From: https://www.spiedigitallibrary.org/conference-proceedings-of-spie on 6/29/2018
Terms of Use: https://www.spiedigitallibrary.org/terms-of-use

Laser Subsystem Parameters		
Number of LGS	5	
LGS locations in field	$(0'', 0'')$ and $(\pm 30'', \pm 30'')$	
Sodium layer range	99 km	
Adaptive Optics Module		
Number of DM's	3	
Conjugate ranges	0.0, 4.5, 9.0 km	
Actuator pitch	$D/16$, $D/16$, $D/8$	
Number of WFS	5 (LGS)	4 (NGS)
WFS order	16 by 16	Tip/tilt
WFS sampling rate	800 Hz	
Control System		
Control algorithm	Minimal variance	
Processing latency + read time	1.25 ms	
-3 dB closed loop bandwidth	32 Hz	

Table 3: MCAO System Simulation Parameters

These parameters were used for the MCAO simulation result presented in this section. D is the telescope aperture diameter (8 meters). These parameters correspond to the Gemini-South MCAO system design, except for the use of 4 instead of 3 NGS tip/tilt guide stars. This modification yields symmetric performance over the 1 arc minute field and simplifies performance evaluation.

Spectral Band	Analysis Strehls			Simulation Strehls		
	Center	Edge	Corner	Center	Edge	Corner
J	0.590	0.478	0.475	0.615	0.509	0.505
H	0.739	0.653	0.649	0.756	0.679	0.674
K	0.843	0.787	0.783	0.854	0.804	0.800

Table 4: MCAO Analysis vs. Simulation Strehl Ratios with Geometric Optics

This table plots mean Strehl ratios at the center, edge, and corner of a square 1 arc minute field of view for the atmospheric and AO system parameters summarized in Tables 2 and 3 above.

Downloaded From: https://www.spiedigitallibrary.org/conference-proceedings-of-spie on 6/29/2018
Terms of Use: https://www.spiedigitallibrary.org/terms-of-use

6 TOWARDS EXTREMELY LARGE TELESCOPES

At first reading, the idea of detailed wave-optics propagation simulations for extremely large telescopes may seem completely impractical. Entry-level proposals for extremely large telescopes such as CELT and GSMT call for roughly a four-fold increase in telescope aperture diameter, implying a 16-fold increase in the number of DM actuators and WFS subapertures even if the number of guide stars, deformable mirrors, and the DM actuator densities are not increased beyond values used for the Gemini-South MCAO design. We are confident that efficient simulations should still be very feasible, however. Significant reductions in the required computer time may actually be possible, assuming that parts of the existing simulation are parallelized and that certain approximations are made in defining the wavefront reconstruction algorithm.

Detailed wave-optics propagation simulations can in fact be less time-consuming and more practical than analytical methods for extremely large telescopes. These propagation simulations converge to typical performance in just a few tens of cycles, since the uncorrectable wavefront error in such systems is, in large part, made up of high spatial frequencies, and the high number of statistically independent variables contributing ensures that the probability of a significant deviation from the long-term average performance is quite small. Calculation of expected performance using analytic methods requires the manipulation of very large non-sparse matrices, and the computational effort required for the necessary matrix operations scales as the cube of the number of WFS subapertures or the sixth power of mirror radius. Since this calculation must typically be repeated for a number of different scenarios, the computation required for an analytic approach is daunting. If we can develop a computationally efficient methods of wavefront reconstruction, as seems likely, propagation simulations are the most practical approach.

Simulation computations may be broken down very generally into (i) wavefront propagation through the atmosphere and optics, (ii) computing the WFS measurements and applying the DM actuator commands, and (iii) deriving the DM actuator commands from the WFS measurements. The computation requirements for part (i) should not be significantly larger for extremely large telescopes, given that the propagation grid size, the number of DM's, and the number of guide stars do not increase dramatically compared with current simulations for 8-meter telescopes. Recent analytical calculations indicate the number of guide stars and DM's necessary for a given level of MCAO performance is a very weak function of telescope aperture diameter, and that good results for 30 meter telescopes should still be possible with only 5 higher-order guide stars and 3 DM's [5]. The propagation grid size for simulations of thirty meter telescopes need not be much greater than 60 meters, provided only that we can assume a turbulence outer scale of about 30 meters. This is only slightly larger than the 50 meter phase screens we are already using for simulations of Gemini-South MCAO. The length of wall clock time required for wavefront propagations could actually be dramatically reduced via parallel computing, since two-dimensional FFT's are easily parallelized. The necessary routines are already available in standard FFT software packages and can be called from MATLAB.

The computation time required to compute WFS measurements and implement DM actuator commands will scale roughly with the total number of WFS subapertures and DM actuators, particularly if the DM actuator pitch is held constant. But these operations represent only a very small fraction of the total calculations for 8 meter simulations, and this would still be true if the number of subapertures and actuators was multiplied by 16.

This is not the case for simulating the wavefront reconstruction algorithm, however. If implemented as an ordinary matrix multiply, the number of computations per wavefront reconstruction scales with the product of the number of DM actuators and WFS subapertures. Scaling the number of actuators and subapertures by a factor of 16 would yield a factor of 256 increase in computation time (and a similar increase in memory), increasing the time spent on this aspect of the simulation from a small fraction of the time required for the wavefront propagations to the largest single contributor. Even worse, the time spent to compute the minimal variance reconstruction algorithm using current methods will scale with the *cube* of the number of WFS subapertures, as it does in the evaluation of analytic models. Much more efficient approaches to wavefront reconstruction that still provide satisfactory performance will need to be developed to efficiently simulate MCAO on extremely large telescopes. Such computationally efficient methods might also be very useful in actual ELT systems.

Downloaded From: https://www.spiedigitallibrary.org/conference-proceedings-of-spie on 6/29/2018
Terms of Use: https://www.spiedigitallibrary.org/terms-of-use

The standard least squares reconstruction algorithm may be implemented very efficiently using sparse matrix methods because the DM-to-WFS influence matrix G is sparse [13]. In the notation of Section 4.6, this reconstructor is defined by the equation

$$\vec{e} = (G^T G)^{-1} G^T \vec{s}. \tag{32}$$

If G is sparse the intermediate quantity $\vec{f} = G^T \vec{s}$ can be computed efficiently, and then the system $(G^T G)\vec{e} = \vec{f}$ can be solved efficiently for $\vec{e}$ by finding an upper/lower triangular factorization for $(G^T G)$ that is also sparse[2]. The number of computations required to prepare this triangular factorization is proportional to the number of actuators to the three-halves power, while estimating the set of actuator commands using this approach scales as the number of actuators multiplied by the natural logarithm of the number of actuators. Unfortunately, simulations to date indicate that this reconstruction approach performs poorly without SVD (singular value decomposition) filtering of poorly sensed modes, and the SVD decomposition of a sparse matrix is not necessarily sparse. It has been suggested that "softer" filtering of the poorly sensed modes using the algorithm

$$\vec{e} = (G^T G + \lambda I)^{-1} G^T \vec{s}, \tag{33}$$

should be considered, since the matrix $(G^T G + \lambda I)$ is no less sparse than $(G^T G)$. More generally, any system of the form $(G^T G + S + L)\vec{e} = \vec{f}$, where S is sparse and L is low rank, can be solved efficiently and could be considered as part of a candidate reconstruction algorithm. These approaches could be first evaluated and optimized in 8-meter simulations, where the optimized minimal variance estimation algorithm is practical to run and can be used as a performance benchmark.

Acknowledgements

This research was supported in part by the Gemini Observatory, which is operated by the Association of Universities for Research in Astronomy, Inc., under a cooperative agreement with the NSF on behalf of the Gemini Partnership: the National Science Foundation (United States), the Particle Physics and Astronomy Research Council (United Kingdom), the National Research Council (Canada), CONICYT (Chile), the Australian Research Council (Australia), CNPq (Brazil), and CONICET (Argentina).

REFERENCES

[1] J.M. Beckers, "Detailed Compensation of Atmospheric Seeing using Multi-Conjugate Adaptive Optics," *SPIE* **1114**, 215–217 (1989).

[2] D.C. Johnston and B.M. Welsh, "Analysis of multiconjugate adaptive optics," *J. Opt. Soc. Am. A* **11**, 394–408 (1994).

[3] B.L. Ellerbroek, "First-order performance evaluation of adaptive-optics systems for atmospheric-turbulence compensation in extended-field-of-view astronomical telescopes," *J. Opt. Soc. Am. A* **11**, 783–805 (1994).

[4] T. Fusco, J.-M. Conan, V. Michau, L.M. Mugnier, and G. Rousset, "Phase estimation for large field of view: application to multiconjugate adaptive optics," *SPIE* **3763**, 125–133 (1999).

[5] B.L. Ellerbroek, "Scaling Multi-Conjugate Adaptive Optics Performance Estimates to Extremely Large Telescopes," *SPIE* **4007**, 1088-1099 (2000).

[6] E.P. Walner, "Optimal wave-front correction using slope measurements," *J. Opt. Soc. Am.* **73**, 1771–1776 (1983).

[2] This can be accomplished by permuting the order of the DM actuators

Downloaded From: https://www.spiedigitallibrary.org/conference-proceedings-of-spie on 6/29/2018
Terms of Use: https://www.spiedigitallibrary.org/terms-of-use

[7] B.M. Welsh and C.S. Gardner, "Effects of turbulence-induced anisoplanatism on the imaging performance of adaptive-astronomical telescopes using laser guide stars," *J. Opt. Soc. Am. A* **8**, 69–80 (1991).

[8] G.A. Tyler, "Merging: a new method for tomography through random media," *J. Opt. Soc. Am. A* **11**, 409–424 (1994).

[9] R. Flicker, B.L. Ellerbroek, and F.J. Rigaut, "Comparison of multiconjugate adaptive optics configurations and control algorithms for the Gemini-South 8m telescope," *SPIE* **4007**, 1032-1043 (2000).

[10] J. Vernin, A. Agabi, R. Avila, M. Azouit, R. Conan, F. Martin, E.Masciadri, L. Sanchez, and A. Ziad, *1998 Gemini Site Testing Campaign: Cerro Pachon and Cerro Tololo*, (Gemini Project, 2000).

[11] J.W. Goodman, *Introduction to Fourier Optics,* McGraw-Hill, New York, 1968.

[12] B.L. Ellerbroek, "A Wave Optics Propagation Simulation for Multi-Conjugate Adaptive Optics," *Beyond Conventional Adaptive Optics,* Venice (in press).

[13] G.M. Cochran, "Sparse Matrix Techniques in Wavefront Reconstruction," Technical Report TR-688, the Optical Sciences Company (1986).

Downloaded From: https://www.spiedigitallibrary.org/conference-proceedings-of-spie on 6/29/2018
Terms of Use: https://www.spiedigitallibrary.org/terms-of-use